Published in *Comp. Mater Sci* **179**, (2020) 109679

Interaction of a mobile {112} grain boundary with radiation induced defects in α-Fe: transformation of defects and impact on the shear-coupled grain boundary migration

Napoleon Anento* and Anna Serra

napoleon.anento@upc.edu, a.serra@upc.edu

Department of Civil and Environmental Engineering, Universitat Politècnica de Catalunya (UPC), Jordi Girona 1-3, 08034 Barcelona, Spain

**Corresponding author*

Abstract

Mobile grain boundaries (GB) may have specific interactions with radiation-induced defects compared with static GBs. In this paper, we consider the GB-defect interactions for the {112} GB that performs shear coupled grain boundary migration mediated by its glissile disconnections. The conservative motion of this GB facilitates the interaction with radiation-induced defects both, mobile and sessile. While mobile defects interact by diffusing to GBs, sessile defects are approached by moving GBs. Clusters at the GB may either be dragged by disconnections or transformed by the motion of the GB that relocates them into the adjacent grain. In turn, the interaction with point defects and their clusters increases the resolved shear stress necessary for the motion of disconnections and subsequent GB migration. The results obtained are directly applicable to the interaction of radiation induced defects with {112} deformation twins.

Key words: Grain boundary - defect interaction, grain boundary mobility, glissile clusters, sessile clusters, MD simulation.

1. Introduction

The properties of irradiated polycrystalline materials under stress, deformation, or temperature are strongly influenced by defect-interface interactions [1]. Grain boundaries (GBs) are known to be sinks for mobile defects, such as point defects and their clusters under irradiation [2, 3]; and they are obstacles for slip systems [4]. The mobility of GBs may be activated by different mechanisms [5] such as GB curvature, thermal effects, ion-induced GB mobility or accommodation of stress [6-11]. Simulation studies have shown that GB-defect interactions can be heterogeneous as a function of the atomic GB structure [3, 12, 13]. These interactions have been object of research mainly focussing on static GBs that interact with mobile defects but little has been reported on the interaction of mobile GBs with radiation-induced defects. This paper focuses on the migration induced by shear, among the possible mechanisms that induce GB mobility.

In irradiated metals, the cluster – GB interaction may occur either because a mobile cluster glides towards the GB or because a mobile GB encounters clusters along its displacement. Migration of grain boundaries with concomitant shear in response to an applied stress occurs by the glide of intrinsic GB dislocations with step character, i.e., disconnections [14-16]. This migration has been observed experimentally [7, 17-21] and studied by computer simulation [21-23]. Since disconnections are GB defects, they can glide only on the GB plane and the motion of the stepped core transforms one crystal at the expenses of the other. An effective source of disconnections in the {112} GB is a sessile GB dislocation that may be created either by the interaction of the pristine GB with a crystal dislocation or by the relaxation of a GB vicinal to the {112} GB. In the latter case, the GB dislocation appears to accommodate the vicinal GBs to be formed by segments of pristine {112} GBs [24]. Stress-driven grain growth at low or intermediate temperature have evidenced the effectiveness of the shear-coupled GB migration among GB-mediated plasticity mechanisms in metals containing both, low- and high-angle GBs [25]. An aspect that has less been explored so far is the interaction of moving GBs with sessile radiation induced defects (RID), which is described in this paper.

Σ3{112} symmetric tilt GBs are commonly observed in ferritic stainless steels [26]. This GB has the lowest energy among the symmetric GBs with <110> tilt axis in bcc metals (the atoms at the GB have the perfect coordination number) [3]. This GB has a special relevance because it is the coherent boundary of the {112} twin, which is the only twin mode in bcc metals [27]. The mobile disconnections of the GB play an essential role in the interaction of the GB with RIDs. The dislocation character of disconnections interacts with RIDs as dislocations in the bulk [28] and the step character of disconnections transforms the structure of defects [29].

Thus, in section 3 we present a detailed description of disconnections in the {112} GBs. In section 4 we present the results of the interaction of the GB with RIDs and the effect of RIDs in the GB migration. Finally, in section 5 we summarize these results.

2. Modelling method

The atomic simulations have been performed using Molecular Statics (MS) and Molecular Dynamics (MD) techniques. The EAM interatomic potential describing Fe was developed by Ackland *et al.* (A04 in [30]). This potential is specially fitted to reproduce point defect properties obtained from *ab initio* calculations and has proven to be able to reproduce accurately the most relevant properties of radiation-induced defects. The accuracy of the potential in the study of tilt <110> GBs was checked in [31].

The simulations are performed in a model consisting of a bi-crystal obtained by applying a tilt about the [110] axis. The misorientation angle is $\theta = 70.53°$ [3]. The crystallographic axes *x, y, z* are oriented along $x = [\bar{1}11]$, $y = [\,110]$ and $z = [\bar{1}1\bar{2}]$ directions. Periodic boundary conditions are applied along *x* and *y* and fixed boundary conditions along *z*. The boundaries in the *z* direction are made of rigid blocks that can move on the *x* and *y* directions to apply shear strains to the system. The thickness of the upper and lower

blocks is 10 nm, which is 2 times the range of the interatomic potential used in this study. The dimensions of the crystal in nm (14.5 x 8.9 x 14.7) where chosen to ensure a negligible effect of rigid boundaries on the interaction processes studied.

To create the disconnection in the GB, the two crystals are stepped along a translation vector as shown in fig.1a and a dislocation is introduced in the bicrystal with the core centred at the step [32, 33]. Finally, to restore periodic boundary conditions along x direction, broken by the introduction of the step, a small rotation about the tilt axis is applied to the whole bicrystal [33]. The glide of the disconnection induces the displacement of the GB in the direction normal to the GB. To move the disconnection we applied a shear strain on the rigid boundaries of the simulated system. The model is suitable to investigate the Peierls stress for disconnection motion under static conditions (T = 0 K) and dynamic properties as a function of shear stress at T > 0 K [34, 35].

The defects considered in this study are point defects, namely vacancy (Vac) and self-interstitial atom (SIA); small clusters of point defects: vacancies (2Vac), mobile interstitials clusters (2, 7, 19 and 61SIA) and sessile interstitial clusters with a C15 Laves phase structure (C15 hereafter). According to DFT results, C15 clusters show the lowest energy configurations [36]; these clusters are formed directly in displacement cascades [37].

The interaction energy, $E_I(A, GB)$ between each of those defects (A) and the GB is calculated according to the following expression:

$$E_I(A, GB) = [E_T(A, GB) - E_T(r = \infty)] \quad (1)$$

Where $E_T(A, GB)$ is the energy of the complex A-GB and $E_T(r = \infty)$ is the energy of the system when the defects A and GB are far enough to be non-interacting. According to this definition, a negative value for $E_I(A, GB)$ implies an attractive interaction between defects A and GB. The binding energy is defined as: $E_b(A, GB) = -E_I(A, GB)$.

Two different defect analysis have been used in the GB-defect interaction. The Wigner-Seitz (WS) method and the analysis of the coordination number (CN).

3. Identification of disconnections

The topological theory of interface defects shows that the Burgers vector of a disconnection is the difference between symmetries of each crystal that are broken when the bicrystal is formed [14, 16]. The Burgers vector of a disconnection with a step formed by n planes parallel to the GB plane is $\overrightarrow{b_n} = \vec{t}_\lambda - \vec{t}_\mu$, where $\vec{t}$ are translation vectors of white (λ) and black (μ) crystals respectively that conform the step, as shown in fig. 1a. The Burgers vectors of disconnections can be easily identified by means of the dichromatic pattern (DP) [38]. The DP of a GB is created by superimposing the lattices of the white (λ) and black (μ) crystals with the GB plane in coincidence, as shown in fig. 1b, so that $\vec{t}_\lambda$ and $\vec{t}_\mu$ have a common origin and the Burgers vector of any possible disconnection is represented by an arrow from black to white lattice sites. The location

of $\vec{b}_n$ in the DP, in relation to the GB, indicates the step high of the disconnection. The unit cells of the crystals are represented by two rectangles in red and blue. Three black arrows in fig. 1b are drawn as examples of possible Burgers vectors. The disconnections $\vec{b}_{\pm 1}$ (above and below the GB) are the ones found experimentally ($\vec{b}_1$ is shown in fig. 4b); the disconnection b_2 is unstable and decomposes into two single steps corresponding to two $\vec{b}_1$.

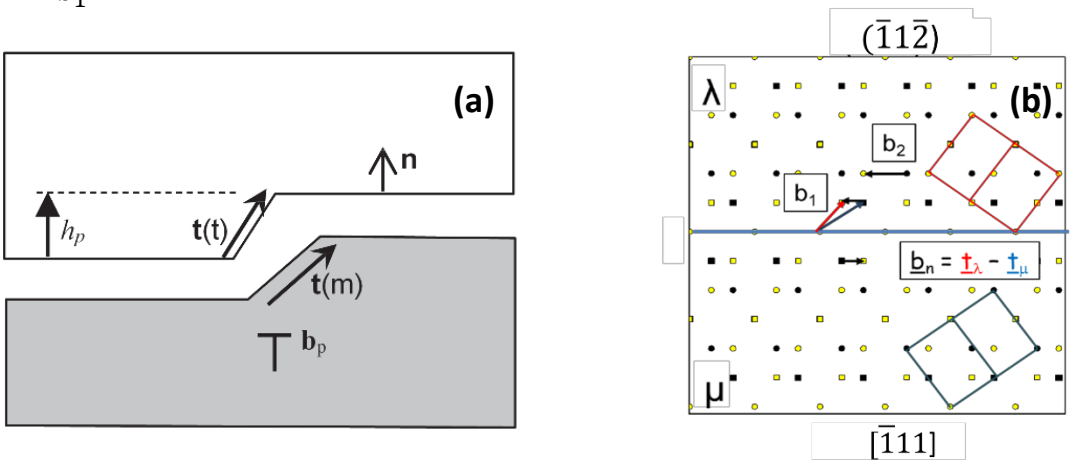

Figure 1. a) Scheme showing the translation vectors of white and black crystals associated to the step of the interface. b) Dichromatic pattern of the {112} tilt grain boundary. Black arrows show Burgers vector of possible disconnections. Red and blue arrows represent the translation vectors of white and black crystals respectively.

The $\vec{b}_1$ disconnection is related to the translation vectors $\vec{t}_\lambda = \frac{1}{2}[111]$ of the upper crystal and $\vec{t}_\mu = [010]$ of the lower crystal. The corresponding Burgers vector is $\vec{b}_1 = 0.167[\bar{1}11]$ parallel to the GB. Dipoles of $\vec{b}_{\pm 1}$ are created under stress, even athermally, because of its small Burgers vector and small step high. Moreover, the disconnection core transforms one crystal into the other during gliding without the need of extra shuffling of atoms [39]. The disconnection $\vec{b}_1$ is responsible for the conservative displacement of the GB.

4. Results and discussion

The $\sum 3\,[110]\ (\bar{1}1\bar{2})$ symmetric tilt GB has a dense atomic structure. The local environment of Fe atoms at the GB is a distorted eight coordination, relatively similar to that in bulk. This would explain the low GB energy (260mJ/m^2) and moderate cluster binding energy as shown in tables 1 and 2. The most stable configuration is shown in fig. 2a. Vacancies and interstitials are trapped at the GB, however, there is no cluster absorption. Even though, there are significant interactions of the GB with interstitial clusters related to the displacement of the GB due to the motion of disconnections. It follows the description of the static properties (binding energies) and the interactions of disconnections with defects that influence the configuration and properties of defects as well as the GB mobility by increasing the resolved shear stress of the disconnections. The stresses, being calculated at 0K, represent an upper bound of the stresses at finite

temperature. Nevertheless, the main processes occurring at the GB during the interactions and the relative influence of the defects in the motion of the disconnections are properly described.

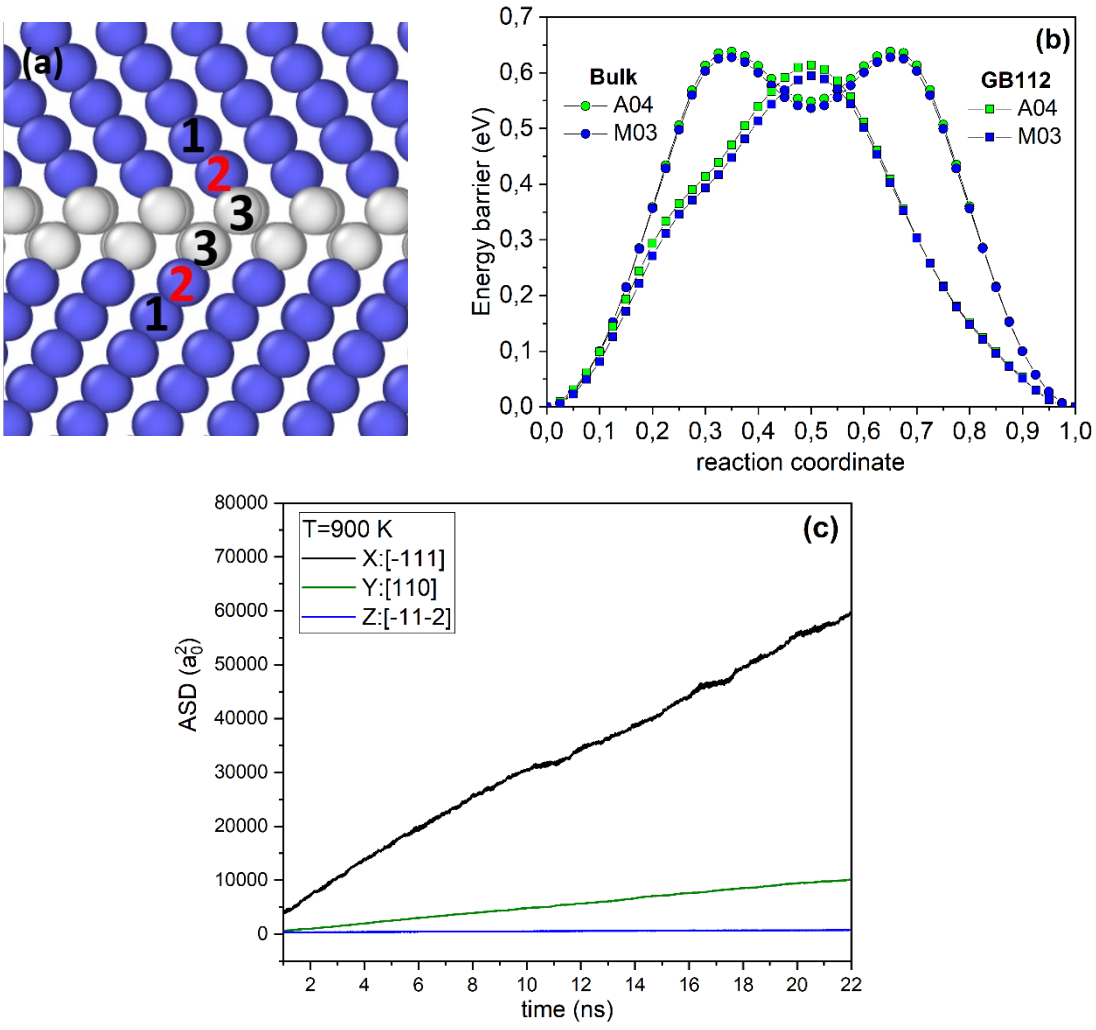

Figure 2. a) Cross section of the GB showing the atomic structure and the sites where the vacancy is located for the calculation of the binding energy; a unit cell is drawn in the lower crystal. b) Vacancy migration barrier in bulk and in the (112) GB. c) Atomic square displacement (for the X, Y and Z components) of a vacancy diffusing along the (112) GB at 900K.

4.1. Point defects at the static {112} GB

Point defects have a positive binding energy with the GB, as shown in Table 1. The interactions with the GB are short-ranged, they decay rapidly at the second and further neighbours of the atoms that form the GB with $E_b < 0.05$ eV. Fig. 2a shows the locations of the vacancy. The maximum binding energy of a vacancy is at sites #2, i.e., above and below the interface ($E_b(2)= 0.18$ eV; $E_b(3)= 0.08$ eV; $E_b(1)= - 0.01$ eV). The di-vacancies with first nearest neighbour (nn) structure that have the stronger interaction with the GB are located at positions #2-2 with $E_b(2\text{-}2)= 0.33$ eV, followed by two di-vacancies with

2nd nn structure at #2-3 with E_b(2-3)= 0.22 eV and at # 3-3 with E_b(3-3)= 0.15 eV respectively. Mono-vacancies and di-vacancies have quite close values of migration energies (~0.63 eV) [40, 41]. The activation energy for dissociation, i.e., the sum of the vacancy migration barrier in the matrix and the binding energy with the GB being about ~0.8 eV and ~1 eV for mono and di-vacancies respectively, implies that detrapping of both defects from the GB has very low probability to occur.

Since there is only one compact <111> direction in the GB ($[\bar{1}11]$ in our simulation), the diffusion of the single vacancy along it is dominant. At 600K, during 20ns, there is a 1-D diffusion with an estimation of jump frequency higher than in bulk. This is in accordance with the decrease of the vacancy migration barrier in the GB ΔE_m = -0.03 eV as compared with the bulk (fig. 2b). At 900K and 1200K, the vacancy can jump along the [110] direction and perform a two-dimensional motion along the GB with predominant jumps along the $[\bar{1}11]$ direction. This is shown in fig. 2c where the atomic square displacement in each direction is plotted versus time. The negligible displacement along the direction perpendicular to the GB shows the confinement of the vacancy in the GB.

There are two stable configurations for the single SIA located at the GB, i.e., [110] dumbbell along the tilt axis and $[\bar{1}11]$ crowdion. The dumbbell configuration has slightly lower energy, i.e., $\Delta E_{<111>-<110>} \sim 0.08$ eV; however, at finite temperature the $[\bar{1}11]$ crowdion configuration is dominant. As a result, single SIAs perform a 1D diffusion within the GB along $[\bar{1}11]$. Thus, at temperatures up to 600K both, vacancy and SIA, perform 1-D diffusion in parallel lines and the probability of recombination would be very low, i.e., the GB would be a neutral sink. At higher temperatures, vacancies perform a 2D diffusion although the predominant direction is still $[\bar{1}11]$ and the GB may be an occasional recombination centre.

Table 1

Point defect	Binding energy PD – {112} GB (eV)	Disconnection unpinning stress (MPa)
1 vacancy	0.18	64
2 vac (1nn, [2-2 in fig. 2a])	0.33	112
2 vac (2nn, [2-3 in fig. 2a])	0.22	75
1 SIA	0.43	115
2 SIAs	0.51	138

Table 1. Binding energy, in eV, of point defects with the {112} GB. Shear stress for the disconnection to overcome the defect.

4.2. Glissile disconnections at the {112} GB: shear coupled GB migration.

Fig. 4a is a scheme of the simulated system with the disconnection and glissile interstitial clusters. Fig. 4b is a cross section of the central part of the simulated system with the GB stepped by the disconnection that moves left under the applied shear stress shown in fig. 4a. The parallel segments of the two lines at the GB give a rough indication of the width of the core, a better estimation of the core is given in the next subsection. The Peierls stress of $\vec{b}_1$ is 20 MPa. The motion of $\vec{b}_1$ allows the displacement of the GB in the direction of its normal. Thus, when the disconnection crosses the periodic boundary conditions, the GB is displaced by one plane. In this way, the GB moves along its normal in the simulated system. The disconnection interacts with other defects located at the vicinity of the GB during its glide and it may transform them, as explained in the following subsections.

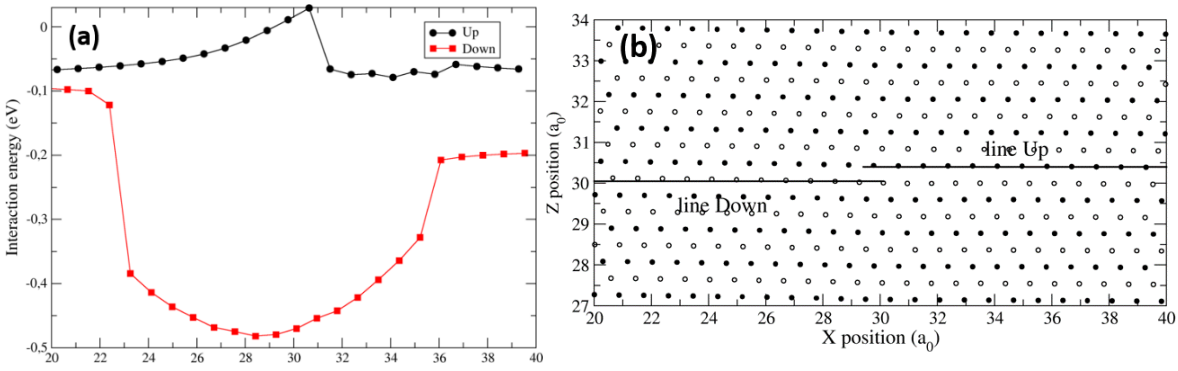

Figure 3. a) Binding energy of a vacancy located at the tension region (black curve) and the compression region (red curve) of a disconnection. b) Cross section of the GB showing the lines where the vacancy is located.

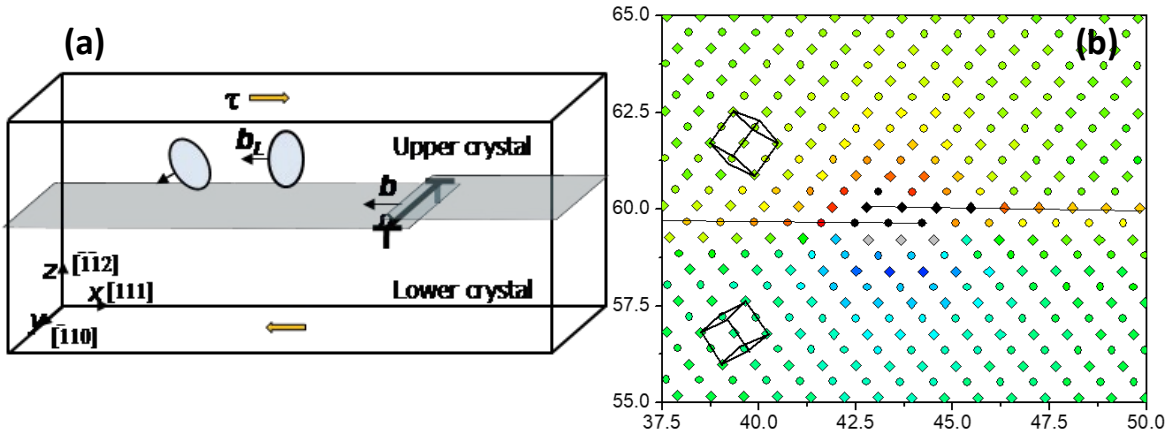

Figure 4: a) Schematic of the simulation box with the disconnection and two clusters. The Burgers vectors of the disconnection and one of the clusters are parallel to the GB, the other cluster has its Burgers vector inclined. The applied shear stress is shown by arrows at the top and bottom of the box. b) Cross section of the simulated system. The unit cells of the two crystals and the location of the GB are indicated.

4.3. Interaction of a gliding disconnection with point defects and mobile clusters

The binding energy of a vacancy with the GB varies in the presence of a disconnection. There is an increase/decrease of the binding energy when the vacancy is at the compression/tension part of the disconnection core, due to the dislocation character of the disconnection. Fig. 3a presents the values of the interaction energy ($-E_b$) for a vacancy located along the planes above and below the glide plane of the disconnection respectively. The two points of discontinuity of the red curve (compression) indicate the extension of the core of the disconnection, which is about 10 lattice parameters (2.9 nm). Notice that the values at the right part of the curve correspond to the points #2 (see fig. 2a) whereas on the left they correspond to the points #3 due to the step of the GB.

Point defects at the GB act as obstacles for the motion of disconnections. The maximum shear stress to unpin the disconnection from an SIA is almost twice the unpinning stress from a vacancy, as shown in Table1. At 0K, when the GB is displaced along its normal by the glide of a disconnection, point defects initially lying at the GB are left behind.

We assume that clusters formed by parallel $< 111 >$ crowdions are identified by Burgers vectors $\vec{b} = \frac{1}{2} < 111 >$. In this sense, glissile $< 111 >$ SIA clusters have their Burgers vectors either parallel or inclined to the {112} GB. Due to the one-dimensional motion of these clusters, only inclined clusters can approach the GB. Table 2 presents the binding energy of all studied clusters with the {112} GB and the range of the interaction that depends on the size and geometry of the considered defect, varying from 0.5 nm up to 2.3 nm. Since the {112} GB can easily move by means of the $\overrightarrow{b_1}$ disconnection, the interaction with both, mobile and sessile clusters, is effective. It should be noted that the length of the disconnection line in the simulation box is 8.9 nm. Therefore, due to the periodic boundary conditions along the disconnection line, there are obstacles interacting with the disconnection separated by 8.9 nm. This fixes the curvature of the disconnection line and therefore the stresses reported in tables 1 & 2 [42]. All simulations have been done at T=0K applying incremental shear strains of 10^{-5} followed by the relaxation of the system.

Table 2

Point defect cluster	Binding energy Cluster - (112) GB (eV)	Max shear stress to transform or drag a defect (MPa)	Range of interaction (distance from GB to cluster in nm)
C15_I_2	0.58	165	0.6
C15_I_3	0.55	220	0.6
C15_I_4	0.85	197	0.5
7SIA parallel	2.11	170 (drag)	0.6
7SIA _Inclined	2.11*	170* (drag)	0.7
19SIA_parallel	4.1	240 (drag)	1.5
19SIA_Inclined	1.3	268	1.1
61SIA_parallel	4.58	260 (drag)	2.3
61SIA_Inclined	1.89	385	1.6

*Table 2. Binding energy, in eV, of mobile (7, 19 and 61SIA) and sessile (C15) clusters with the (112) GB. Shear stress necessary to drag glissile clusters and to transform sessile clusters. (*During motion towards GB it reorients parallel to the GB). Range of interaction GB-defect.*

4.3.1. Interaction of a gliding disconnection with a cluster formed by crowdions parallel to the GB

In this case, the Burgers vector of the cluster is parallel to the Burgers vector of the disconnection; figs. 5a and 5c present two examples. These clusters can perform a 1-D motion parallel to the GB but cannot approach it. In this study, the GB has migrated towards the edge of the cluster by successive displacements along its normal due to the glide of the disconnection. In this situation, the disconnection that moves by the effect of an external shear stress is attracted and finally pinned by the cluster. This is indicated by the left part of plots in fig. 5b that shows the initial drop of stress (attraction of the disconnection by the cluster) followed by the increase of the stress due to the pinning of the disconnection. The process is repeated each time the disconnection passes near the cluster. The increase of the maximum unpinning stresses at each pass of the disconnection indicates that the binding with the cluster increases because the distance to the GB decreases. The disconnection starts dragging the cluster when its binding energy is high enough, which depends on the size of the cluster. Thus, the 7SIA and 19SIA are dragged when three interstitials are at the GB, whereas the 61SIA cluster is dragged when the first interstitial is at the GB (see fig. 5c). As explained above, a single interstitial at the GB is stable in crowdion configuration and perform a 1-D motion, therefore the crowdions of the periphery of the cluster that are at the GB can glide easily along the GB when the cluster is dragged by the disconnection. Notice that the distance from the cluster to the glide plane of the disconnection, i.e. the GB, is small compared to the corresponding drag distance of edge dislocations in the bulk [43]. The right part of the stress-strain curves in fig. 5b shows the constant stress necessary for the drag of three clusters (260 MPa for the 61SIA cluster, 240 MPa for 19SIAs and 170 MPa for the 7SIAs). Thus, due to the drag of clusters there is an increase of the shear necessary to produce shear-coupled GB migration. In this case, the cluster is neither absorbed nor transformed. For these clusters to be swept by the GB, i.e. relocated by the action of the disconnection to the other side of the boundary, it is necessary that they are pinned, for instance when decorated by solute atoms [44, 45].

4.3.2. Interaction of a gliding disconnection with a cluster inclined relative to the GB

Clusters of 7, 19 and 61SIA with crowdion lines intersecting the GB are attracted and move towards the GB from a distance of 1nm at T=0K. The GB captures these clusters although there is no absorption. During the motion towards the GB, 7SIA clusters spontaneously reorient to a more stable position parallel to the GB; this reorientation occurs even at T=0K. Once at the GB, the 7SIA cluster performs a 1D motion along the $[\bar{1}11]$ direction and it is dragged by the disconnection. 19 and 61SIA clusters do not

reorient, at least at T=0K. When a disconnection meets the first interstitial of the cluster it relocates the interstitial into the adjacent grain. This process is repeated each time a disconnection meets the remaining of the cluster up to its total transformation. The interstitials relocated at the adjacent crystal form a new cluster with the crowdions parallel to the GB, which is the most stable configuration. This reorganization can only be completed when all interstitials are detached from the GB, which implies that for the 19 and 61SIA clusters there is no drag of the new created cluster at the other side of the GB unless the stress is reversed and the GB moves again towards the cluster. The maximum shear stress for the total transformation of the 19SIA and 61SIA cluster is 268MPa and 385 MPa respectively.

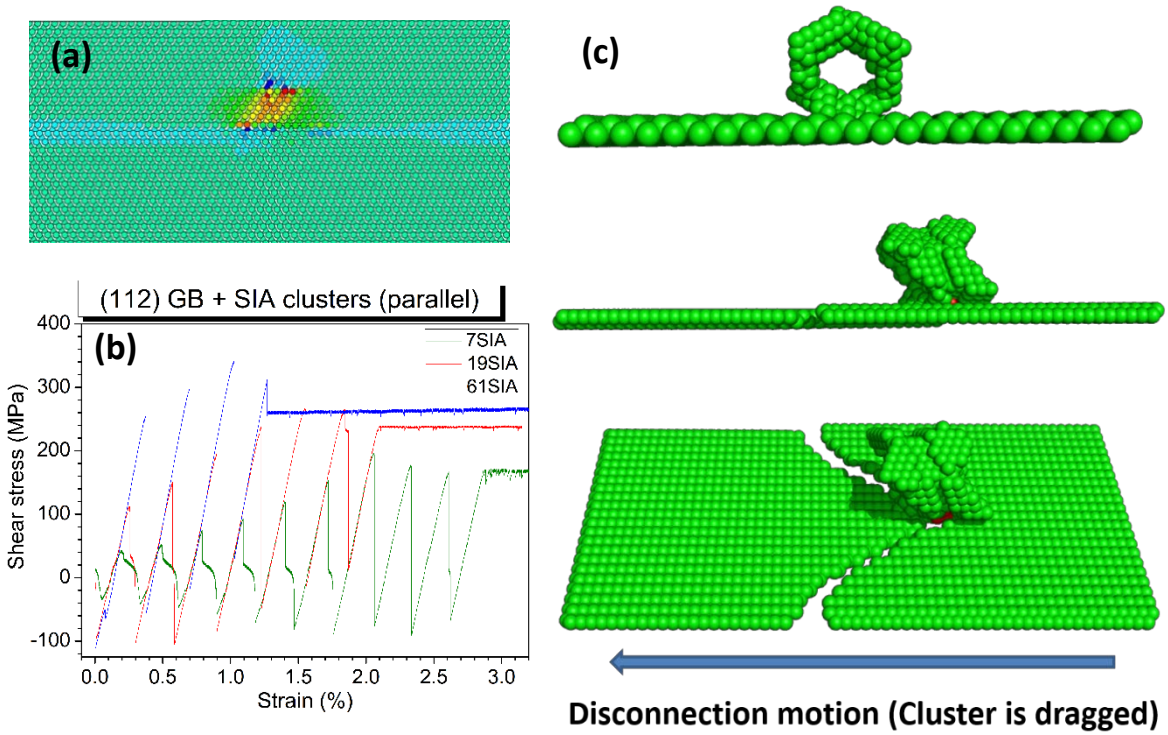

Figure 5: a) Pressure map of a cross section showing the GB tangent to a cluster with Burgers vector parallel to the GB; green indicates compression and blue tension. b) stress-strain curves showing the repeated passes of the disconnection (left part of curve) and drag of clusters (right part of curve). c) three perspectives of a dragged 61SIA cluster: view along the Burgers vector, view perpendicular to the Burgers vector and view of the disconnection dragging the cluster. Image 5c obtained from CN analysis. (See on line version for coulored figure)

4.4. Interaction of a gliding disconnection with sessile clusters.

Clusters may be sessile either because of its structure, such as C15, or because they have been decorated by impurities. In both cases, the interaction with the gliding disconnections of the GB transform them from one crystal to the other. C15, formed by 2, 3 and 4 interstitials, transform in clusters of parallel dumbbells that are mobile.

Fig. 6a shows how the disconnection is first attracted and then pinned by the C15_I_2 cluster. For a given position of the GB, the shear stress has three stages, depending on the position of the disconnection (fig. 6b): the stress coincides with the Peierls stress when the disconnection does not interact with the cluster; then, the stress decreases by the attraction of the cluster and, finally, it increases up to the unpinning of the disconnection. Each cycle of the stress-strain curve corresponds to the passage of the disconnection when the GB is at a certain distance of the cluster. The maximum of each cycle depends on the distance of the GB to the cluster. The maximum stress for the total transformation is indicated in table 2.

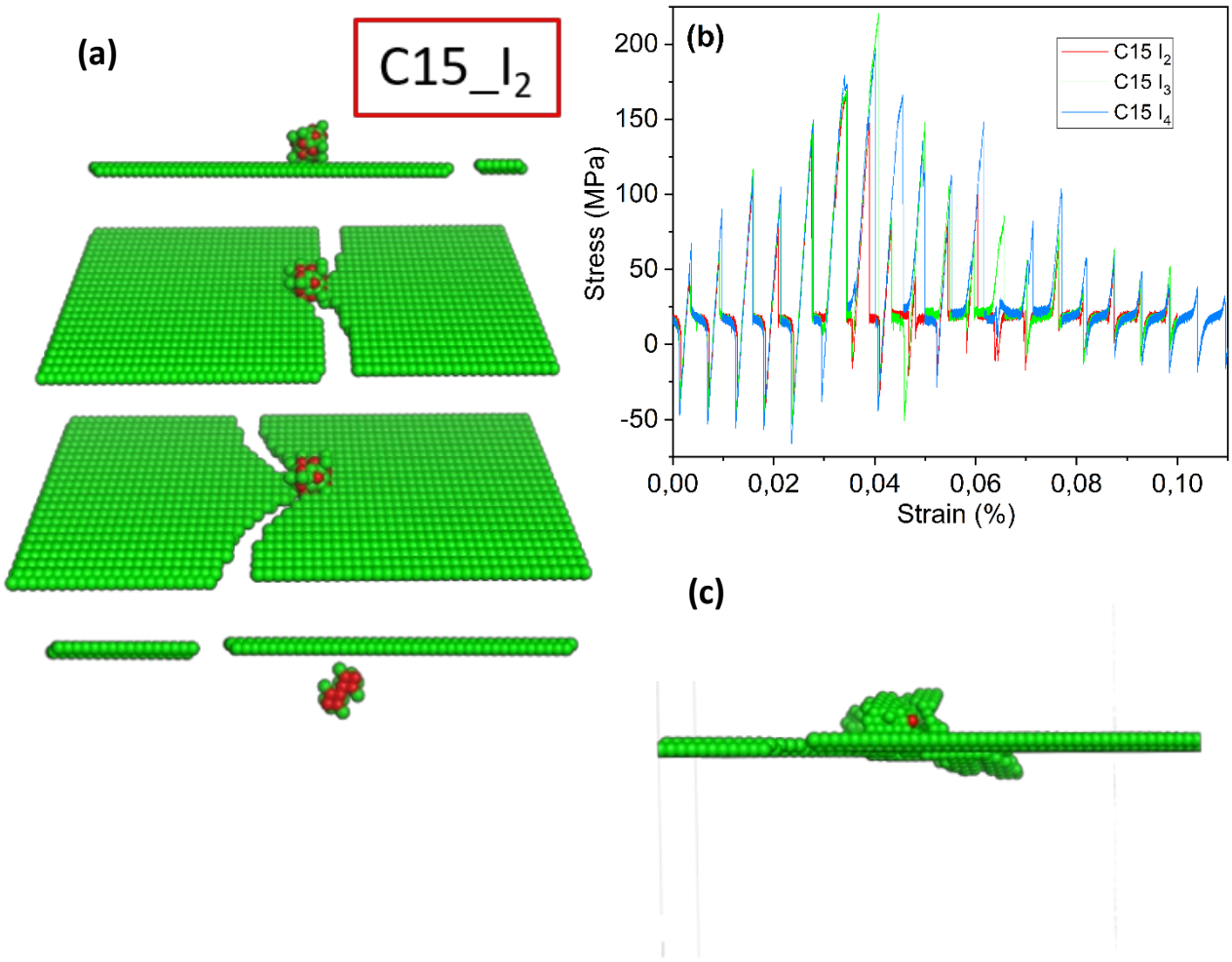

Figure 6: a) Four snapshots showing a C15 (I2) before, during and after its transformation by the disconnection (moving from right to left). The two intermediate images show the disconnection attracted and pinned respectively by the defect. b) Stress-strain curve initiated when the GB was well below the cluster and finished when the GB was well above the new cluster formed by parallel dumbbells. c) Interaction of the {112} GB with a cluster located at the upper crystal and immobilized by a carbon atom. Part of the cluster is already in the lower crystal.

Clusters with Burgers vector parallel to the GB that have been pinned by a solute atom (a carbon atom in our simulation) are immobile and cannot be dragged, thus they are transformed into clusters at the adjacent grain by the same mechanism as the inclined clusters. The result is a cluster with a Burgers vector parallel to the GB located in the adjacent crystal; fig. 6c shows the initial stage of transformation. The carbon atom remains attached to the cluster after the complete transformation.

5. Concluding remarks

The {112} <110> tilt grain boundary performs a conservative shear induced motion (shear coupled GB migration) due to the glide of disconnections, which are GB line defects with both, dislocation and step character. The displacement of the GB allows its interaction with radiation-induced defects both, mobile and sessile. The interaction is mediated by gliding disconnections. In turn, defects are obstacles for the motion of disconnections, increasing their resolved shear stress; consequently, increasing the stress necessary for the displacement of the GB and accommodation of plastic deformation. It follows the description of the studied processes taking place at this GB.

- Vacancies and self-interstitials are trapped at the {112} GB. Both point defects diffuse one dimensionally along the single <111> direction of the GB. Moving in parallel directions, their recombination is marginal, i.e., the {112} GB is a neutral sink for point defects. At T≥ 900K, the vacancy can jump sporadically along the [110] direction, slightly increasing the recombination with interstitials. On the other hand, point defects are obstacles for the motion of {112} GB disconnections.
- The {112} GB does not absorb interstitial clusters but strongly interact with them.
- The interactions of the {112} GB with clusters formed by parallel crowdions characterized by Burgers vectors $\vec{b} = \frac{1}{2} < 111 >$ are as follows:
    - The disconnections at the {112} GB drag interstitial clusters with Burgers vector parallel to the GB.
    - The {112} GB attracts clusters with Burgers vectors inclined to the GB. Once they are at the GB, the successive sweep of disconnections transform these clusters from one grain to the other and reorient the cluster with a new Burgers vector parallel to the GB. The same transformation occurs to clusters with Burgers vector parallel to the GB that are immobilized by impurities.
- The successive glide of disconnections transforms three-dimensional sessile clusters with a C15 Laves phase structure, created in cascades, into mobile clusters formed by <110> interstitials.
- The interaction of mobile {112} GBs with interstitial clusters keeps the number of interstitials of the clusters but changes their structure, trajectory and, sometimes, mobility.
- The presence of defects produced by irradiation increases the stress necessary to move disconnections at the GB affecting the shear-coupled GB migration associated to the {112} GB.

- There is only one deformation twin type in Fe, i.e., the {112} twin. Therefore, all conclusions described above are applicable to the {112} twin boundaries. This implies that radiation induced defects affect twinning in the sense that it is needed a higher stress to move the twinning disconnections responsible for the growth and shrinkage of twins.

Thus, the {112} GB does not absorb but transform clusters produced during irradiation. In turn, the presence of point defects and interstitial clusters near {112} GBs contributes to the increase of the flow stress of plastic deformation.

Disclosure statement

The authors reported no potential conflict of interest. This publication reflects only the author's view and the Commission is not responsible for any use that may be made of the information it contains.

Acknowledgements

This project has received funding from the Euratom research and training programme 2014-2018 under grant agreement No 661913 (SOTERIA). This work also contributes to the Joint Program on Nuclear Materials (JPNM) of the European Energy Research Alliance (EERA). The research has been partially supported by the Spanish MINECO (FIS2015-69017-P).

Data availability

The processed data required to reproduce these findings cannot be shared at this time as the data also forms part of an ongoing study

References

1. I.J. Beyerlein, M.J. Demkowicz, A. Misra, B.P. Uberuaga, Progress Mater. Sci. 74 (2015) 125
2. G.S. Was, Fundamentals of Radiation Materials Science: Metals and Alloys, 1st ed. (Berlin: Springer, 2007).
3. M. A. Tschopp, K. N. Solanki, F. Gao, X. Sun, M. A. Khaleel, and M. F. Horstemeyer, Phys. Rev. B 85 (2012) 064108
4. T.R. Bieler, P. Eisenlohr, C. Zhang, H.J. Phukan, M.A. Crimp, COSSMS, 18 (2014) 212
5. A.P. Sutton and R.W. Balluffi, Interfaces in Crystalline Materials, Oxford Classic Series 2006 (Oxford University Press, New York, NY, 1995)
6. G. Gottstein and L.S. Shvindlerman, Grain Boundary Migration in Metals: Thermodynamics (Kinetics: Applications, CRC Press, Boca Raton, 2009).
7. T. Rupert, D. Gianola, Y. Gan, and K. Hemker, Science 326 (2009) 1686

8. C. Braun, J.M. Dake, C.E. Krill, and R. Birringer, Sci. Rep. 8 (2018) 1592
9. J. Han, S.L. Thomas, and D.J. Srolovitz, Prog. Mater. Sci. 98 (2018) 386
10. K. D. Molodov, D. A. Molodov, Acta Mat, 153 (2018) 336
11. C. M. Barr, O. El-Atwani, D. Kaoumi, K. Hattar, JOM, 71 (2019) 1233
12. X.-M. Bai, A.F. Voter, R.G. Hoagland, M. Nastasi, and B.P. Uberuaga, Science 327 (2010) 1631.
13. A. Dunn, R. Dingreville, E. Martínez, and L. Capolungo, Acta Mater. 110 (2016) 306.
14. R. C. Pond, in Dislocations in Solids, F.R.N. Nabarro Editor, North-Holland, Vol. 8, (1989) 1
15. J.P. Hirth, R.C. Pond, Acta Mater., 44 (1996) 4749.
16. R.C. Pond and J. P. Hirth, Solid St. Phys., 47 (1994) 287.
17. T.Gorkaya, D.A. Molodov, G. Gottstein, Acta Mater 57 (2009) 5396.
18. T.Gorkaya, T. Burlet, D.A. Molodov, G. Gottstein, Scripta Mater, 63 (2010) 633.
19. T.Gorkaya, K.D. Molodov, D.A. Molodov, G. Gottstein, Acta Mater, 59 (2011)5674.
20. K.D. Molodov, T. Al-Samman, D.A. Molodov, S. Korte-Kerzel, Acta Mater. 134 (2017) 267
21. T. Braisaz, P. Ruterana, G. Nouet, A. Serra, Ph. Komninou, Th. Kehagias and Th. Karakostas, Philos Mag Letters, 74 (1996) 331.
22. H.A. Khater, A. Serra, R.C. Pond, J.P. Hirth, Acta Mater. 60 (2012) 2007
23. A. Ostapovets, A. Serra, Philos Mag, 94 (2014) 2827.
24. P.L. García-Müller, N. Kvashin, N. Anento and A. Serra, (2019) Submitted for publication
25. D.A. Molodov, T.Gorkaya, G. Gottstein, J. Mater Sci, 46 (2011) 4318
26. H. Beladi , G. S Rohrer, Acta Materialia 61 (2013) 1404
27. J.W. Christian and S. Mahajan, Prog. Mater. Sci. 39 (1995) 1
28. Yu.N. Osetsky, D.J. Bacon, F. Gao, A. Serra, B.N. Singh, J. Nuc. Mater. 283-287 (2000) 784
29. R.C. Pond, J.P. Hirth, A.Serra, D.J. Bacon, Mater Res Letters, 4 (2016) 185
30. G.J. Ackland, M.I. Mendelev, D.J. Srolovitz, S. Han, A.V. Barashev, J. Phys.: Condens. Matter 16 (2004) S2629.
31. D. Terentyev, X. He, A. Serra, J. Kuriplach, Comp. Mater. Sci, 49 (2010) 419
32. Yu.N. Osetsky, D.J. Bacon: Modelling Simul. Mat. Sci. Eng. 11 (2003) 427.
33. A. Serra and D.J. Bacon, Zeitschrift für Metallkunde, 95 (2004) 4.
34. A. Serra and D.J. Bacon, Mater. Sci. Eng., A 400–401 (2005) 496
35. A. Serra, D.J. Bacon, Yu.N. Osetsky, Philos Mag Letters, 87 (2007) 451
36. L. Dezerald, M.C. Marinica, L. Ventelon, D. Rodney, F. Willaime J. Nucl. Mater. 449 (2014) 219
37. M.C. Marinica, F. Willaime, J.P. Crocombette, Phys. Rev. Lett. 108 (2012) 025501.
38. R.C. Pond and D.S. Vlachavas, Proc. of The Royal Society of London, Series A: Mathematical and Physical Sciences 386 (1983) 95
39. H.A. Khater, A. Serra, R.C. Pond, Philos. Mag, 93, (2013) 1279

40. L. Malerba, M.C. Marinica, N. Anento, C. Björkas, H. Nguyen, C. Domain, F. Djurabekova, P. Olsson, K. Nordlund, A. Serra, D. Terentyev, F. Willaime, C.S. Becquart, J. Nuc. Mater., 406 (2010) 19
41. G Bonny, R C Pasianot, L Malerba, Modelling Simul. Mater. Sci. Eng. 17 (2009) 025010
42. Z.Rong, V.Mohles, D.J.Bacon and Yu.N.Osetsky, Philos. Mag., 85 (2005) 171.
43. D.J.Bacon, Yu.N.Osetsky, Z.Rong and K.Tapasa, In: H.Kitagawa and Y.Shibutani (eds) IUTAM Symposium on Mesoscopic Dynamics in Fracture Process and Strength of Materials, 173-182, 2004 Kluwer Academic Publisher.
44. D. Terentyev, N. Anento, A. Serra, V. Jansson, HA Khater, J. Bonny, J. Nucl. Mater. 408 (2011) 272
45. N. Anento and A. Serra, J. Nucl. Mater. 440 (2013) 236